Nanoscale

PAPER

View Article Online
View Journal | View Issue

Cite this: *Nanoscale*, 2014, **6**, 10095

Enhanced radiation therapy with internalized polyelectrolyte modified nanoparticles

Peipei Zhang, Yong Qiao, Chaoming Wang, Liyuan Ma* and Ming Su*

Received 21st March 2014
Accepted 18th May 2014

DOI: 10.1039/c4nr01564a

www.rsc.org/nanoscale

A challenge of X-ray radiation therapy is that high dose X-ray under therapeutic conditions damages normal cells. This paper describes a nanoparticle-based method to enhance X-ray radiation therapy by delivering radio-sensitizing gold nanoparticles into cancer cells. The nanoparticles have been modified with cationic polyelectrolytes to allow internalization. Upon X-ray irradiation of nanoparticles, more photoelectrons and Auger electrons are generated to cause water ionization, leading to formation of free radicals that damage DNA of cancer cells. The X-ray dose required for DNA damage and cell killing is reduced by delivering gold nanoparticles inside cancer cells.

Introduction

X-ray photons in radiation therapy can generate photoelectrons and Auger electrons, which can cause ionization of water and formation of reactive free radicals (mostly hydroxyl radicals). The free radicals diffuse through chain reactions in cells, and damage DNA in mitochondria and nuclei by extracting hydrogen atoms from ribose sugars, leading to cleavage of the polynucleotide backbone.[1–9] A challenge of X-ray radiation therapy is that high dose X-ray can damage normal cells and cause side effects due to its low tumor selectivity.[10] Nanoparticles of gold,[11–13] platinum[14] or bismuth[15,16] have been proposed to enhance radiation therapy, but the measured effect of nanoparticles is negligible.[17–19] This is likely due to the fact that these nanoparticles are attached on the cell membrane, and X-ray generated free radicals have to diffuse into the vicinity of DNA to cause damage.[19] If radiosensitizers could be placed in cancer cells or nuclei, the amount of free radicals available for DNA damage will be enhanced, and the total X-ray dose could be reduced to receive the same treatment effect.[19]

The cell membrane penetrating ability of nanoparticles depends on sizes, shapes and surface properties such as charge and hydrophobicity.[20–23] Nanoparticles that are modified with positively charged molecules can be attracted on the negatively charged cell surface, and taken up by cells *via* endocytosis.[24] Layer-by-layer assembly allows controlled surface modification of nanoparticles by depositing polyelectrolytes of opposite charges.[25] The surface charge of nanoparticles is controlled by the amount of polyelectrolyte adsorbed on the outmost surface, providing a facile and effective way of optimizing the cellular uptake efficiency. This paper describes a new way to enhance X-ray radiation killing of aggressive cancer cells by internalizing gold nanoparticles into cancer cells (Fig. 1A), where alternating cationic and ionic polyelectrolytes are used to modify gold nanoparticles (Fig. 1B). It is found that gold nanoparticles with positive charges show enhanced intracellular delivery into cells and these nanoparticles do not affect cell viability. Upon X-ray irradiation, cells with internalized positively charged gold nanoparticles show a higher level of DNA damage and susceptibility to be killed, compared to the negatively charged nanoparticles that are not internalized.

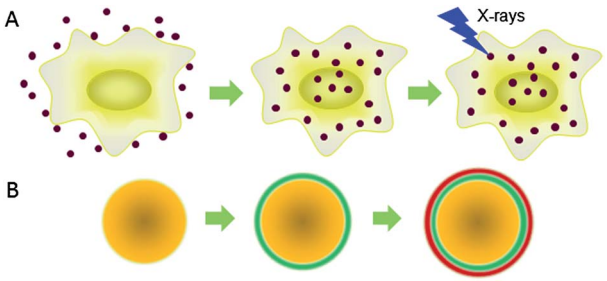

Fig. 1 Cell-penetrating nanoparticles for enhanced X-ray radiation therapy (A); nanoparticles modified with polyelectrolyte multilayers (B).

Experimental section

Polyethylenimine (PEI) (10 000 Da), polysodium 4-styrene sulfonate (PSS) (70 000 Da), and polydiallyl-dimethyl ammonium chloride (PDAC) (100 000–200 000 Da) were from Aldrich. Polydimethylsiloxane (PDMS Sylgard 184) was from Dow-Corning. PDMS stamps were prepared by casting the PDMS pre-polymer and a curing agent on solid masters made by photo-lithography. Rhodamine isothiocyanate (RITC), fluorescein isothiocyanate (FITC), propidium iodide (PI) and gold nanoparticles were from Sigma. SYBR green fluorescence dye was from Invitrogen.

Department of Biomedical Engineering, Worcester Polytechnic Institute Worcester, Massachusetts 01069, USA. E-mail: msu2@wpi.edu; lma2@wpi.edu

PEI was labeled with FITC or RITC by reacting with FITC or RITC in water at a 3000 : 1 molar ratio (PEI repeat units and dye molecules) for 24 h at room temperature. Gold nanoparticles and polyelectrolytes were used at concentrations of 1.0×10^{10} nanoparticles mL^{-1} and 5.0 mg mL^{-1}, respectively. To coat nanoparticles with polyelectrolytes, the nanoparticle suspension was added drop-wise into PEI-RITC solution. The modified nanoparticles were collected by centrifugation, and then added in PSS solution. The steps were repeated until a desired number of layers were formed around nanoparticles. Human glioblastoma cells (A712) were cultured in RPMI 1640 medium supplemented with 10% (v/v) cosmic calf serum, 100 units mL^{-1} of penicillin, and 100 mg mL^{-1} streptomycin at 37 °C and 5% CO_2. Polyelectrolyte modified nanoparticles were added into culture medium at a nanoparticles-to-cell ratio of 100. After incubation for 24 h, cells were washed with phosphate buffered saline (PBS)(1×) to remove excess nanoparticles.

Live dead assay was performed on cells with gold nanoparticles with a LIVE/DEAD® kit (Life Technologies) according to the instructions provided by the company. An Accuri C6 cytometer (BD Bioscience Inc.) equipped with an air-cooled laser (20 mW) at 488 and 640 nm with the standard filter setup was used for flow cytometry assay. For cell cycle analysis, cells were fixed in 3 mL 100% ethanol, and DNAs were stained with 0.4 mL PI (0.5% PI in PBS with 0.1% Trition X-100) and assessed by flow cytometry. The histogram was analyzed by defining borders of different phases of the cell cycle (G0/G1, G2, S, and M). The mean fluorescence intensity (MFI) of cells was measured using the software equipped with the machine. The production of free radicals was assessed with an Image-iT™ LIVE Green Reactive Oxygen Species (ROS) detection kit (Life Technology Inc.) using a fluorescent marker, 5-(-6)-carboxy-2,7-di-chlorodihydro-fluorescein diacetate (carboxy H2 DCFDA), which permeates live cells, and can be deacetylated by non-specific intracellular esterases. The deacetylated fluorogenic marker can generate green color under a fluorescence microscope.

DNA damage was measured using alkaline halo assay.[26] Briefly, cells exposed to X-ray or nanoparticles were patterned to form a single cell array on a glass substrate, and embedded in 0.1% (mass ratio) agarose gel. After gel solidification, the slide was incubated with 0.3 M NaOH for 15 min at room temperature, and stained with 10 μg mL^{-1} SYBR for 10 min. The slide was incubated with deionized water for 3 min to remove excess SYBR. Phase contrast and epi-fluorescence images were collected with 40× and 10× objectives on an inverted microscope (Olympus IX83). DNA double strand break was assessed with expression of a DNA repair protein, ϒ-H2XA. Briefly, A172 cells with different treatments were fixed with 4% paraformaldehyde in PBS for 20 min, and treated with 0.1% Triton X-100 in PBS for 5 min. After incubating in blocking buffer (3% bovine serum albumin in PBS) for 1 h, primary antibodies against ϒ-H2XA were added to cells, and incubated at room temperature for 2 h. After rinsing with PBS, cells were incubated with FITC-conjugated secondary antibody (anti-rabbit IgG-FITC antibody produced in goat) for 1 h, washed with PBS, stained with 0.2 μg mL^{-1} DAPI for 15 min and again washed with PBS. The fluorescence intensity of the secondary antibody labeled cells was measured with a 96 well plate reader under an excitation light of 488 nm (Perkin-Elmer 1420 multilabel counter 1420). Electrophoresis was performed under alkaline conditions, where cells were treated with 0.3 M alkaline solution for 10 min (pH 13).

Results and discussion

Fig. 2A is a transmission electron microscopy (TEM) image of gold nanoparticles, which have an average diameter of 13.5 ± 1.3 nm. The nanoparticles are modified with three layers of polyelectrolytes, *i.e.*, PEI, PSS, and PEI. To confirm the presence of multilayers, two fluorescent dyes, *i.e.*, green colored FITC and red colored RITC are incorporated in the inner-most PEI layer and outmost PEI layer, respectively, as shown in fluorescence microscopy images (Fig. 2B and C). Fig. 2D is a merged image collected with TRITC and FITC filters of the fluorescence microscope. The yellow color confirms the existence of PEI-RITC and PEI-FITC on nanoparticles. The zeta potential of nanoparticles has been measured after addition of each layer (Fig. 2E). A reversal of surface charge following the deposition of each layer is clear. The size distribution of nanoparticles has been tested using dynamic light scattering. The sizes of nanoparticles increase with the number of layers (Fig. 2F). When the number of layers is over 4, the formation of polyelectrolyte bridges (flocculation) between adjacent nanoparticles brings nanoparticles closer, causing large size variation (135 nm) (Fig. 2G). An ultraviolet-visible spectrometer is used to characterize nanoparticles modified with 1 to 5 layers of polyelectrolytes. A red shift of the absorption peak to long wavelengths reflects the deposition of the polyelectrolyte layer, which changes dielectric constants around nanoparticles.

PEI coated positively charged nanoparticles are added into the culture medium of A172 cells. After 24 h, the cell viability test shows that cells are green, indicating cells are alive (Fig. 3A), where red color is from PEI-RITC modified nanoparticles. The location of nanoparticles relative to cells is tested using phase contrast imaging (Fig. 3B) and fluorescent imaging (Fig. 3C).

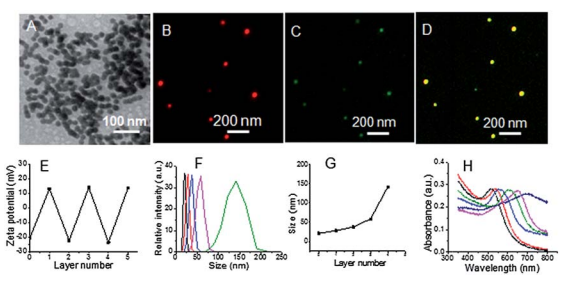

Fig. 2 TEM image of gold nanoparticles (A); fluorescence images of nanoparticles under a TRIC (B) and FITC filter (C); merged picture of images collected with a TRIC and FITC filter (D); zeta potential (E) and dynamic light scattering (F) results of nanoparticles after addition of each polyelectrolyte layer; the maximum size of polyelectrolyte modified nanoparticles (G); UV-vis spectra of nanoparticles after adding each layer of polyelectrolytes (H).

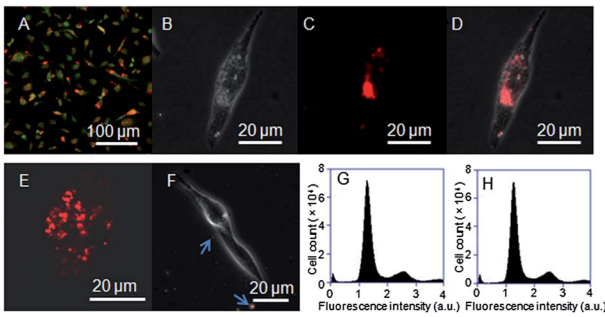

Fig. 3 Live/dead assay of cells with nanoparticles (A); phase contrast (B) and fluorescence (C) images of cells with nanoparticles; merged phase contrast and fluorescence images (D); confocal fluorescence image of cells with nanoparticles in the z stack at 7.5 μm under the cell surface (E); interaction of negatively charged nanoparticles with A 172 cells (F); flow cytometry analysis of the cell cycle of cells without nanoparticles (G) and with nanoparticles (H).

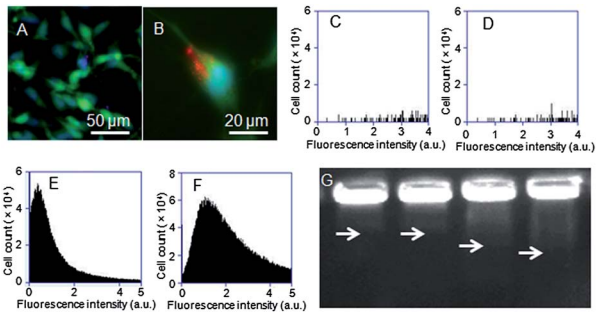

Fig. 4 Fluorescence image (A) and an enlarged image (B) of ROS stained cells that have internalized nanoparticles; flow cytometry results: cells with (C) and without (D) internalized nanoparticles without X-ray; cells without (E) and with (F) internalized nanoparticles with X-ray; gel electrophoresis results of four samples (bands from left to right are from sample 1 to sample 4) (G).

The merged image indicates that nanoparticles are adjacent to cells (Fig. 3D). To determine whether nanoparticles are internalized in cells or not, the cells have been imaged at a focal length of 7.5 μm using a confocal microscope. Fig. 3E shows that some nanoparticles are in the same focus plane. The fluorescence image indicates that 92.8% of cells have internalized nanoparticles. The fluorometry result shows that ~81 nanoparticles are internalized in each cell. In comparison, negatively charged nanoparticles with PSS at the outmost layer are not taken up by cells at all (Fig. 3F), where no nanoparticles can be found inside cells, and the arrows show nanoparticles left after washing. In order to determine whether internalized nanoparticles affect the cell cycle, cells with and without internalized nanoparticles are stained with propidium iodine (PI) and analyzed by flow cytometry. Fig. 3G and H show a similar distribution in cell number-fluorescent intensity plots of both samples: 72.3% cells with internalized nanoparticles and 71.9% cells without internalized nanoparticles are in G0/G1, suggesting that internalization does not change cell cycles.

The production of free radicals in cells after X-ray irradiation (40 kV, 100 μA, and 80 mGy min^{-1}) is indicated in a fluorescence image using a carboxy H2 DCFDA probe. Fig. 4A shows strong green fluorescence emission and a high level of free radicals from cells with internalized charged nanoparticles. An enlarged image shows the co-existence of fluorescently labelled nanoparticles (red color), DAPI stained nucleus (blue), and free radical generated green fluorescence from each cell (Fig. 4B). Flow cytometry is used to quantify free radicals in four sets of samples: cells with negatively charged (1) or internalized (2) nanoparticles; cells with negatively charged nanoparticles and X-ray (3); cells with internalized nanoparticles and X-ray (4). Fig. 4C and D show that there is almost no detectable fluorescence signal from samples (1) and (2). MFI in sample (4) (5.0×10^6) is 3 times stronger than that in sample (3) (1.6×10^6) (Fig. 4E and F). DNA damages in the four samples are assessed by electrophoresis, where cells are treated with 0.3 M NaOH for 10 min, and DNAs are stained with ethidium bromide (EB). DNA damages are quantified by distances that DNA fragments move in gel electrophoresis. Fig. 4G shows that DNAs in samples (1) and (2) have moved a similar distance, indicating that DNA damage levels in both samples are similar. DNAs from X-ray irradiated cells with internalized nanoparticles move a longer distance than those from cells without internalized nanoparticles.

DNA damage in each sample has been quantified using PI stained DNAs as a marker using flow cytometry. Cells in different phases have different amounts of DNA: normal cells in the G0/G1 phase have 1 unit of the DNA content; those in the S phase have an increased DNA content due to duplication; upon entering the G2 phase and later the M phase, the DNA content is doubled (2 units). Cells are irradiated with X-ray for 15 minutes, and put back to incubator for 48 h. The fluorescence intensity corresponding to no DNA damage is set at 1 unit; those lower than 1 unit is caused by either apoptosis or DNA damaged into smaller fragments. Fig. 5A and B show flow cytometry results of X-ray irradiated cells with negatively charged nanoparticles and internalized nanoparticles, respectively. 38.8% cells with negatively charged nanoparticles and 72.4% cells with internalized nanoparticles show a fluorescence intensity below 1 unit, suggesting that internalized nanoparticles can enhance X-ray induced DNA damage. Fig. 5C shows the MFI of each sample: cells with negatively charged nanoparticles (1.38×10^6), cells with internalized nanoparticles alone (1.38×10^6), cells with negatively charged nanoparticles and X-ray (1.25×10^6), and cells with internalized nanoparticles and X-ray (0.82×10^6). Cell death (apoptosis) after different treatments has also been

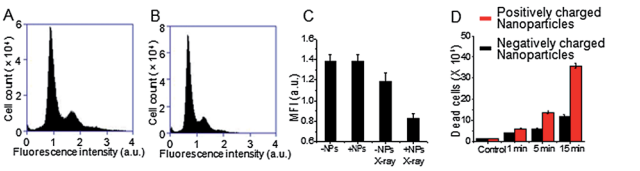

Fig. 5 X-ray induced DNA damage of cells with negatively charged (A) and internalized (B) nanoparticles; MFI of cells after different treatments (C); apoptosis cell counting (D).

determined using flow cytometry. A specific number of cells (10^6) with internalized positively charged nanoparticles are exposed to X-ray irradiation for different times, and cultured in medium for 48 h. Dead cells that float up in medium are collected, enriched by centrifugation, stained with PI, and counted by flow cytometry. As the irradiation time increases from 0, 1, 5, to 15 min, more cells are killed (Fig. 5D). Cells with negatively charged nanoparticles and X-ray are tested as comparison, where fewer cells are killed even when radiation conditions are the same

DNA damage has been assessed at single cell level using HaloChip assay.[26] Briefly, cells after different treatments are attached on a solid substrate to form a single cell array, and embedded in an agarose gel. After gel solidification, the sample is immersed in an aqueous solution of NaOH for lysis. Damaged DNA fragments will self-diffuse into the gel matrix, forming a diffusive ring around nucleus. After staining cells with SYBR dye, DNA damage is quantified with relative nuclear diffusion factor (rNDF), which is derived from areas of halo and nucleus as follows:

$$\mathrm{rNDF} = (R^2 - r^2)/r^2$$

where R and r are the radii of halo and nucleus, respectively. Fig. 6A–D show the fluorescence images of four samples, where each image (A–D) is from each sample (1–4). Fig. 6E shows rNDFs of cells after different treatments, where cells with internalized nanoparticles and X-ray irradiation have an rNDF of 4.52 ± 0.18, which is larger than those of cells with negatively charged nanoparticles (1.47 ± 0.08), cells with internalized nanoparticles (1.51 ± 0.10), and cells with negatively charged nanoparticles and with X-ray (2.41 ± 0.07). At last, DNA double strand break has been assessed with expression of a DNA repair protein, γ-H2AX. Primary and fluorescent labeled secondary antibodies are added sequentially into culture media, and cells are imaged with a fluorescence microscope. Fig. 6F–I show the fluorescence images of four samples, where each image (F–I) is from each sample (1–4). Cells with negatively charge nanoparticles (Fig. 6F) and internalized nanoparticles (Fig. 6G) show no fluorescence signal, indicating that almost no γ-H2AX is expressed. Cells with negatively charged nanoparticles and X-ray show a low level of fluorescence (Fig. 6H). Cells with X-ray and internalized nanoparticles show an increased fluorescence signal (Fig. 6I), indicating an increased expression of γ-H2AX.

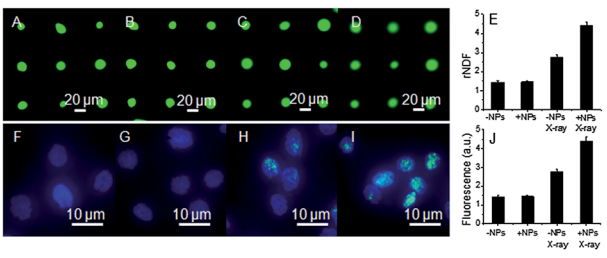

Fig. 6 Fluorescence images of four samples after HaloChip assay (A–D), and their rNDFs (E); immuno-staining of the γ-H2AX protein in four samples (F–I) and the corresponding fluorescence intensity (J).

The expression of the γ-H2AX protein is quantified with a 96 plate reader under an excitation light of 488 nm. Fig. 6J shows that cells with nanoparticles and X-ray show 170% higher intensity than those treated with X-ray alone, indicating enhanced DNA damage.

Conclusions

A nanoparticle-based method is developed to enhance the X-ray dose in radiation therapy by internalization of polyelectrolyte modified nanoparticles into cancer cells. Gold nanoparticles modified with positively charged polyelectrolytes have shown higher cell membrane penetrating ability than those with negatively charged ones. The internalized nanoparticles do not change the cell cycle, and can enhance X-ray radiation treatment of cancer, causing more DNA damage and cell death compared to those with negatively charged nanoparticles.

Acknowledgements

This project is supported by a Director's New Innovator Award from the National Institute of Health (1DP2EB016572).

Notes and references

1 F. Mark, U. Becker, J. N. Herak and D. Schultefrohlinde, *Radiat. Environ. Biophys.*, 1989, **28**, 81–99.
2 G. Pratviel, J. Bernadou and B. Meunier, *Angew. Chem., Int. Ed.*, 1995, **34**, 746–769.
3 W. K. Pogozelski and T. D. Tullius, *Chem. Rev.*, 1998, **98**, 1089–1107.
4 C. Chatgilialoglu and P. O'Neill, *Exp. Gerontol.*, 2001, **36**, 1459–1471.
5 M. Dizdaroglu, P. Jaruga, M. Birincioglu and H. Rodriguez, *Free Radical Biol. Med.*, 2002, **32**, 1102–1115.
6 S. S. Wallace, *Free Radical Biol. Med.*, 2002, **33**, 1–14.
7 C. Borek, *J. Nutr.*, 2004, **134**, 3207s–3209s.
8 B. F. Godley, F. A. Shamsi, F. Q. Liang, S. G. Jarrett, S. Davies and M. Boulton, *J. Biol. Chem.*, 2005, **280**, 21061–21066.
9 A. Akar, H. Gumus and N. T. Okumusoglu, *Appl. Radiat. Isot.*, 2006, **64**, 543–550.
10 Z. Goldberg and B. E. Lehnert, *Int. J. Oncol.*, 2002, **21**, 337–349.
11 J. F. Hainfeld, D. N. Slatkin, T. M. Focella and H. M. Smilowitz, *Br. J. Radiol.*, 2006, **79**, 248–253.
12 T. Kong, J. Zeng, X. P. Wang, X. Y. Yang, J. Yang, S. McQuarrie, A. McEwan, W. Roa, J. Chen and J. Z. Xing, *Small*, 2008, **4**, 1537–1543.
13 S. J. McMahon, W. B. Hyland, M. F. Muir, J. A. Coulter, S. Jain, K. T. Butterworth, G. Schettino, G. R. Dickson, A. R. Hounsell, J. M. O'Sullivan, K. M. Prise, D. G. Hirst and F. J. Currell, *Radiother. Oncol.*, 2011, **100**, 412–416.
14 E. Porcel, S. Liehn, H. Remita, N. Usami, K. Kobayashi, Y. Furusawa, C. Le Sech and S. Lacombe, *Nanotechnology*, 2010, 21.
15 M. Alqathami, A. Blencowe, U. J. Yeo, R. Franich, S. Doran, G. Qiao and M. Geso, *J. Phys.: Conf. Ser.*, 2013, 444.

16 Y. Luo, M. Hossain, C. M. Wang, Y. Qiao, J. C. An, L. Y. Ma and M. Su, *Nanoscale*, 2013, **5**, 687–694.
17 B. L. Jones, S. Krishnan and S. H. Cho, *Med. Phys.*, 2010, **37**, 3809–3816.
18 E. Lechtman, N. Chattopadhyay, Z. Cai, S. Mashouf, R. Reilly and J. P. Pignol, *Phys. Med. Biol.*, 2011, **56**, 4631–4647.
19 M. Hossain and M. Su, *J. Phys. Chem. C*, 2012, **116**, 23047–23052.
20 N. L. Rosi, D. A. Giljohann, C. S. Thaxton, A. K. R. Lytton-Jean, M. S. Han and C. A. Mirkin, *Science*, 2006, **312**, 1027–1030.
21 D. A. Giljohann, D. S. Seferos, P. C. Patel, J. E. Millstone, N. L. Rosi and C. A. Mirkin, *Nano Lett.*, 2007, **7**, 3818–3821.
22 C. B. He, Y. P. Hu, L. C. Yin, C. Tang and C. H. Yin, *Biomaterials*, 2010, **31**, 3657–3666.
23 M. D. Massich, D. A. Giljohann, A. L. Schmucker, P. C. Patel and C. A. Mirkin, *ACS Nano*, 2010, **4**, 5641–5646.
24 E. C. Cho, J. W. Xie, P. A. Wurm and Y. N. Xia, *Nano Lett.*, 2009, **9**, 1080–1084.
25 G. Decher, *Science*, 1997, **277**, 1232–1237.
26 Y. Qiao, C. M. Wang, M. Su and L. Y. Ma, *Anal. Chem.*, 2012, **84**, 1112–1116.